Preprints of the 19th World Congress
The International Federation of Automatic Control
Cape Town, South Africa. August 24-29, 2014

Novel Reciprocal Self-Sensing Techniques for Tapping-Mode Atomic Force Microscopy

Michael G. Ruppert * and **S. O. Reza Moheimani** *

* *School of Electrical Engineering and Computer Science, The University of Newcastle, Callaghan, NSW 2308, Australia*
Michael.Ruppert@uon.edu.au; Reza.Moheimani@newcastle.edu.au

Abstract: We evaluate two novel reciprocal self-sensing methods for tapping-mode atomic force microscopy (TM-AFM) utilizing charge measurement and charge actuation, respectively. A microcantilever, which can be batch fabricated through a standard microelectromechanical system (MEMS) process, is coated with a single piezoelectric layer and simultaneously used for actuation and deflection sensing. The setup enables the elimination of the optical beam deflection technique which is commonly used to measure the cantilever oscillation amplitude. The voltage to charge and charge to voltage transfer functions reveal a high amount of capacitive feedthrough which degrades the dynamic range of the sensors significantly. A feedforward control technique is employed to cancel the feedthrough and increase the dynamic range from less than 1 dB to approximately 30 dB. Experiments show that the conditioned self-sensing schemes achieve an excellent signal-to-noise ratio and can therefore be used to provide the feedback signal for TM-AFM imaging.

1. INTRODUCTION

In atomic force microscopy (AFM) (Binnig et al., 1986) high-resolution images can be obtained by mapping the intermolecular forces between a microcantilever with a sharp tip and a sample's surface. Tapping-mode (Zhong et al., 1993) AFM emerged as a popular method to minimize lateral friction forces in order to enable imaging of soft biological samples by exciting the cantilever near its first resonance frequency. This comes at the cost of low scan speeds due to constraints set by the bandwidth of the z-axis feedback loop and the transient response of the cantilever. Extensive research has been conducted on Q-Control (Mertz et al., 1993) to increase scan speed, but other methods such as scanning on higher eigenmodes (Ruppert et al., 2013) or decreasing the size of the cantilever (Walters et al., 1996) have also been proposed.

Silicon cantilevers have proven to be very suitable for tapping-mode AFM and additionally they can be manufactured economically using microfabrication processes (Albrecht et al., 1990). Even with sophisticated actuation techniques such as photothermal (Yamashita et al., 2007), magnetic (Han et al., 1996) or ultrasonic actuation (Yamanaka and Nakano, 1996) these cantilevers are usually excited at their base by means of a dither piezoelectric transducer, which introduces additional unwanted actuator dynamics. As most commercial AFM systems rely on displacement measurement obtained with the optical beam deflection technique (Meyer and Amer, 1988), an appropriate laser position on the cantilever becomes crucial but might not be obtained at all, especially for small cantilevers. Additional drawbacks of this method arise from possible optical interference and optical feedback (Kassies et al., 2004) and contribute to the measurement noise.

Ultimately, the size and cost of the AFM system could be greatly reduced with integrated sensors or self-sensing techniques. An integrated piezoresistive element in the silicon cantilever instrumented with a Wheatstone bridge (Tortonese et al., 1993) enables near sensorless strain measurement but requires an additional coating of doped silicon. When a piezoelectric layer is deposited on one side of the cantilever, piezoelectric sensing (Itoh and Suga, 1993) can be used to estimate the cantilever deflection by measuring the electrical current flowing through the piezoelectric material. Recently, alternative methods such as tunnel magnetoresistive sensing (Tavassolizadeh et al., 2013) have been proposed that promise high bandwidth and resolution but require the generation of a homogeneous magnetic field which complicates the design. Cantilevers with thermal heating loops located at the tip for actuation and a piezoresistive element at the cantilever base for sensing (Fantner et al., 2009) have also been suggested but major control effort to compensate for coupling has to be employed.

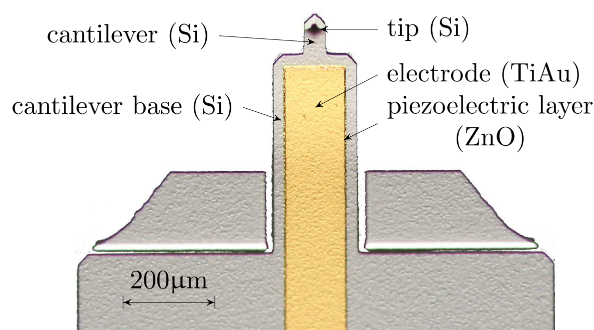

Fig. 1. Image of the piezoelectric microcantilever.

Copyright © 2014 IFAC

In previous work (Ruppert and Moheimani, 2013), the authors have demonstrated charge sensing and signal conditioning using a combination of analog circuitry and a Field Programmable Analog Array (FPAA) for a cantilever shown in Fig. 1. The cantilever suffices with a single piezoelectric layer for both actuation and sensing. This contribution proposes two reciprocal self-sensing techniques using a charge measurement circuit and a charge drive circuit to effectively extract an estimate of the cantilever's deflection without the optical laser sensor. Capacitive feedthrough cancellation is systematically obtained over a band of frequencies around the resonance with the use of a feedforward controller. In Section 2 the equivalent electromechanical actuator and sensor model of the cantilever is discussed. The resulting transfer functions from applied actuator voltage to measured charge and from applied charge to measured voltage contain a significant amount of feedthrough, decreasing the dynamic range. In Section 3 and Section 4 the system properties and the analog circuitry to realize the reciprocal self-sensing techniques are presented. In Section 5 the self-sensing signals are compared with the laser signal with respect to signal-to-noise ratio and scan experiments are shown which validate the applicability of the self-sensing techniques to be used for topography estimation.

2. OPEN-LOOP MODEL OF THE SELF-SENSING PIEZOELECTRIC CANTILEVER

By bonding a piezoelectric layer to the surface of a cantilever, a transducer with inherent self-sensing capabilities is obtained. As can be seen in the schematic shown in Fig. 2a the piezoelectric layer (ZnO) is bonded on the tip side of the cantilever between two electrodes (TiAu). Assuming perfect bonding between the piezoelectric transducer and the beam, a voltage applied to the electrodes results in a bending moment causing the cantilever to deflect. The transfer function relating the actuator voltage $V(s)$ to cantilever deflection $D(s)$, only considering the fundamental mode, is given by (Moheimani and Fleming, 2006)

$$G_{dv}(s) = \frac{D(s)}{V(s)} = \frac{\alpha\omega_0^2}{s^2 + 2\zeta\omega_0 s + \omega_0^2}. \quad (1)$$

Similarly, when a piezoelectric transducer is subjected to mechanical strain it becomes electrically polarized, producing a charge on the surface of the material. This direct piezoelectric effect can be modeled as a strain dependent voltage source V_p in series with a capacitor

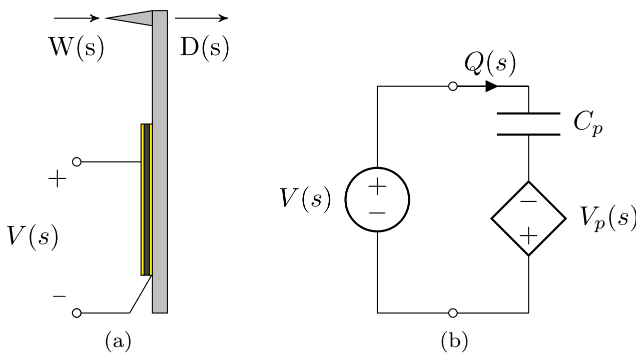

Fig. 2. (a) Simplified schematic and (b) equivalent electrical circuit model of the piezoelectric cantilever.

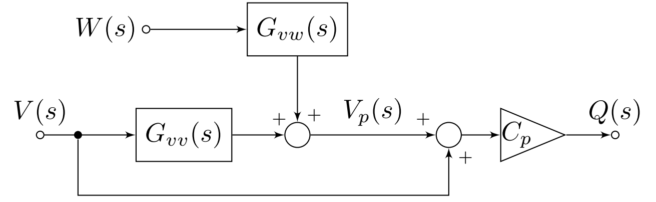

Fig. 3. Blockdiagram representing the transfer function from voltage actuation and tip disturbance to charge in the piezoelectric material.

C_p as shown in Fig. 2b. While the capacitor sufficiently represents the dielectric properties of the piezoelectric material, this simplified model does not take into account dielectric losses or heat dissipation which can be modeled by adding a resistor in parallel to V_p and C_p. The model is a simplified version of the Butterworth Van Dyke model as proposed by the IEEE Standard on Piezoelectricity (Meitzler et al., 1988). The piezoelectric voltage V_p can be modeled as the linear combination of the direct excitation voltage $V(s)$ and a voltage due to the disturbance input at the cantilever tip $W(s)$

$$V_p(s) = G_{vv}(s)V(s) + G_{vw}(s)W(s) \quad (2)$$

with

$$G_{vv}(s) = \frac{\beta\omega_0^2}{s^2 + 2\zeta\omega_0 s + \omega_0^2} \quad \text{and} \quad (3)$$

$$G_{vw}(s) = \frac{\delta\omega_0^2}{s^2 + 2\zeta\omega_0 s + \omega_0^2}. \quad (4)$$

Applying Kirchhoff's law to Fig. 2b, one obtains

$$V(s) = \frac{1}{C_p}Q(s) - V_p(s). \quad (5)$$

Substituting (2) into (5) yields

$$Q(s) = \left[C_p + C_p G_{vv}(s)\right]V(s) + C_p G_{vw}(s)W(s), \quad (6)$$

which is illustrated in the block diagram in Fig. 3.We note that the charge in the piezoelectric layer depends on the excitation voltage and the disturbance input but most importantly is dominated by a feedthrough term $C_pV(s)$. Consequently, the disturbance will remain unnoticed in the charge output if the feedthrough is large. Furthermore, $G_{vw}(s)$ cannot be measured directly. Thus we focus on the system

$$G_{qv}(s) = \frac{Q(s)}{V(s)} = C_p + C_p G_{vv}(s). \quad (7)$$

to demonstrate the effect of the feedthrough. Observing that (1) and (3) only differ by a constant factor, (7) can be rewritten as

$$G_{qv}(s) = C_p + C_p\gamma G_{dv}(s). \quad (8)$$

From (8) we conclude that by exciting the cantilever with a voltage and measuring the charge, a deflection estimate of the cantilever can be obtained if the feedthrough term $C_pV(s)$ can be canceled. In addition, it is reasonable to ask whether the inverse also holds true, i.e. does the voltage across the piezoelectric layer serve as a deflection estimate when the cantilever is driven by a charge source? For this purpose the voltage source in Fig. 2b is replaced by a charge source and (5) is solved for the piezoelectric voltage V_p. Using

$$V(s) = G_{vv}^{-1}(s)V_p(s), \quad (9)$$

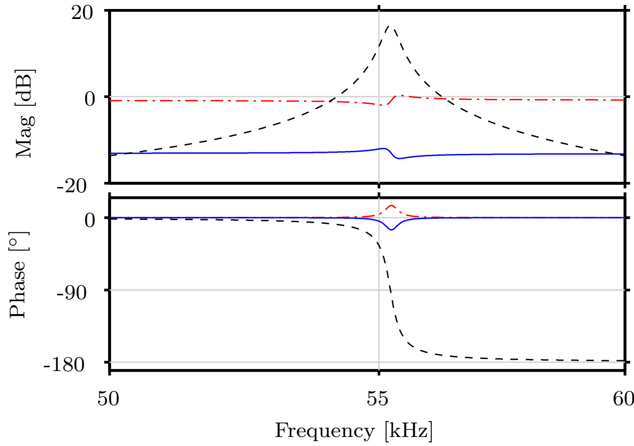

Fig. 4. Simulated frequency responses of G_{dv} (−−), G_{qv} (−) and G_{vq} (−·−). G_{qv} and G_{vq} have been scaled to show the dynamics in a single plot. The parameters used are $\alpha = 0.04\,\mu\mathrm{m/V}$, $\omega_0 = 2\pi 55.2\,\mathrm{kHz}$, $\zeta = 0.003$, $C_p = 22\,\mathrm{pF}$ and $\gamma = 0.04$.

the transfer function from charge actuation to piezoelectric voltage, neglecting the disturbance $W(s)$, is found to be

$$G_{v_p q}(s) = \frac{V_p(s)}{Q(s)} = \frac{1}{C_p}\frac{G_{vv}(s)}{1+G_{vv}(s)}. \qquad (10)$$

Inherent to the structure of the system is that the transfer function contains a unity feedback path which shifts the resonance frequency of $G_{vv}(s)$. Since $V_p(s)$ cannot be measured directly, the voltage across the Piezo $V(s)$ has to be used instead. By substituting (3) in (10) or simply inverting (7), the transfer function from charge actuation to $V(s)$ is found to be

$$G_{vq}(s) = \frac{V(s)}{Q(s)} = \big(G_{qv}(s)\big)^{-1} = \frac{1}{C_p}\frac{1}{1+\gamma G_{dv}(s)}. \qquad (11)$$

Both transfer functions, $G_{qv}(s)$ and $G_{vq}(s)$, show feed-through terms of C_p and ${C_p}^{-1}$, respectively. It remains the task of the signal conditioning to remove the feedthrough terms which degrade the dynamic range significantly. In Fig. 4 the simulated frequency responses from actuation voltage $V(s)$ to displacement $D(s)$ (as measured with the standard laser method) and to charge $Q(s)$ as well as from charge actuation to voltage across the piezoelectric terminals for typical values are shown. It can be seen that the capacitive feedthrough terms heavily bury the resonance peak which leads to a poor dynamic range of around 1 dB as opposed to 30 dB achieved with the laser sensor. As TM-AFM relies on mapping amplitude variations induced by the shift of the resonance frequency, systems such as $G_{qv}(s)$ and $G_{vq}(s)$ would not be suitable for imaging. The following sections will introduce the necessary signal conditioning to remove the feedthrough and recover good estimates for the cantilever displacement.

3. VOLTAGE ACTUATION - CHARGE SENSING

3.1 System Properties

Let the input to the system $u(t)$ be the voltage across and the output of the system $y(t)$ be the charge on the piezoelectric layer as in Fig. 2b. Then the derivative of the output (current flowing through the piezoelectric layer) is the dual of the input in the sense that $u(t)\dot{y}(t)$ is equal to the power provided by the system. Such a system is negative imaginary (NI) and the transfer function $G_{qv}(s)$ satisfies the negative imaginary property, i.e. it is stable and satisfies (Petersen and Lanzon, 2010)

$$j\big[G(j\omega) - G^*(j\omega)\big] \geq 0 \qquad \forall \omega > 0. \qquad (12)$$

Indeed, it can be shown that if $G_{dv}(s)$ is negative imaginary

$$j\big[G_{dv}(j\omega) - G^*_{dv}(j\omega)\big] = \frac{4\alpha\zeta\omega_0^3\omega}{(\omega_0^2-\omega^2)^2+(2\zeta\omega_0\omega)^2} > 0,$$

then $G_{qv}(s)$ is also negative imaginary

$$j\big[G_{qv}(j\omega) - G^*_{qv}(j\omega)\big] = \frac{4C_p\gamma\alpha\zeta\omega_0^3\omega}{(\omega_0^2-\omega^2)^2+(2\zeta\omega_0\omega)^2} > 0,$$
$$\text{with} \quad C_p, \gamma, \alpha, \zeta, \omega_0, \omega > 0.$$

This property is advantageous when charge is used for feedback control in order to change the cantilever Q-factor. From (Petersen and Lanzon, 2010) it is known that a negative imaginary system in positive feedback with a strictly negative imaginary controller will result in closed loop stability if a DC-gain condition is satisfied. The resonant controller (Moheimani and Fleming, 2006) and positive position feedback controller (Fanson and Caughey, 1990) are two examples of strictly negative imaginary controllers, which can provide a high level of damping (Fairbairn and Moheimani, 2012; Ruppert et al., 2013).

3.2 Charge Sensing

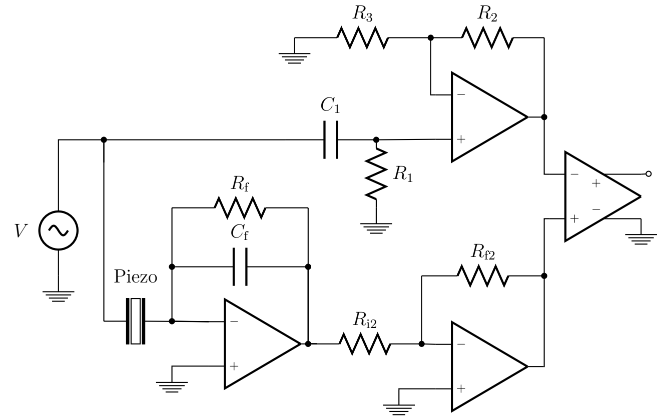

Fig. 5. Simplified circuit diagram of piezoelectric cantilever in the voltage driven - charge measured setup.

A charge mode amplifier, which represents the lower branch of the circuit shown in Fig. 5, is used to measure the charge in the piezoelectric transducer while a voltage signal at resonance is applied. The first stage amplifier will equate the charge present at its negative input terminal by charging the feedback capacitor C_f. A feedback resistor R_f is used to prevent the amplifier from drifting into saturation. A second stage inverting amplifier is used to accommodate for the inverting character of the first stage and to provide additional gain. The transfer function of the two stages is then given by

$$H_{qv}(s) = \frac{as}{s+\omega_c}, \qquad (13)$$

resembling a high-pass filter with a low frequency cut-off at $\omega_c = (R_f C_f)^{-1}$ and a gain of $a = R_{f2}(R_{i2}C_{f1})^{-1}$. The values are chosen such that the frequency of interest (the resonance frequency of the first eigenmode of the cantilever) lies well within the bandwidth of the charge sensor.

3.3 Feedthrough Cancellation

Fig. 6 reveals that a feedforward controller of the form

$$K(s) = C_p H_{qv}(s) \tag{14}$$

based on the piezoelectric capacitance of the cantilever and the transfer function of the charge measurement circuit can be derived to cancel the feedthrough term. The circuit shown in Fig. 5 incorporates the charge amplifier stage and a non-inverting high-pass filter resembling the feedforward controller. An instrumentation amplifier is employed to cancel the feedthrough and to amplify only the strain related signal.

4. CHARGE ACTUATION - VOLTAGE SENSING

4.1 System Properties

With $G_{qv}(s)$ being NI and invertible, $G_{vq}(s)$ will be positive imaginary (PI), i.e.

$$j\left[G_{vq}(j\omega) - G_{vq}^{*}(j\omega)\right] = j\left[G_{qv}^{-1}(j\omega) - G_{qv}^{-*}(j\omega)\right] =$$
$$= -\frac{4C_p\gamma\alpha\zeta\omega_0^3\omega\left[(\omega_0^2-\omega^2)+(2\zeta\omega_0\omega)^2\right]}{a^2+(2C_p\gamma\alpha\zeta\omega_0^3\omega)^2} < 0$$

with

$$a = C_p\left[(\omega_0^2-\omega^2)^2+(2\zeta\omega_0\omega)^2\right] + C_p\gamma\alpha\omega_0^2(\omega_0^2-\omega^2),$$
$$C_p, \gamma, \alpha, \zeta, \omega_0, \omega > 0.$$

As it is characteristic for a negative imaginary system that its phase response lies between 0° and −180°, the phase response of its inverse will lie between 0° and 180°. A key observation is that if $G_{vq}(s)$ is augmented with an integrator, which is equivalent to rotating the Nyquist plot by −90°, a positive real (PR) system is obtained. Furthermore, the negative feedback interconnection of a PR system and a strictly positive real (SPR) system is again PR and therefore stable (Brogliato et al., 2007, chap. 2). Based on this result, the application of a simple integral controller of the form

$$C_I(s) = \frac{k}{s}, \qquad k > 0 \tag{15}$$

in unity negative feedback with $G_{vq}(s)$ will achieve damping with favorable stability and robustness properties. This was previously demonstrated for a nanopositioning stage with force actuators and force sensors (Fleming, 2010).

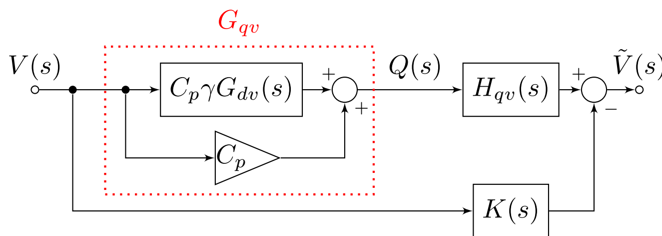

Fig. 6. Block diagram showing the schematic setup of charge measurement and feedthrough cancellation.

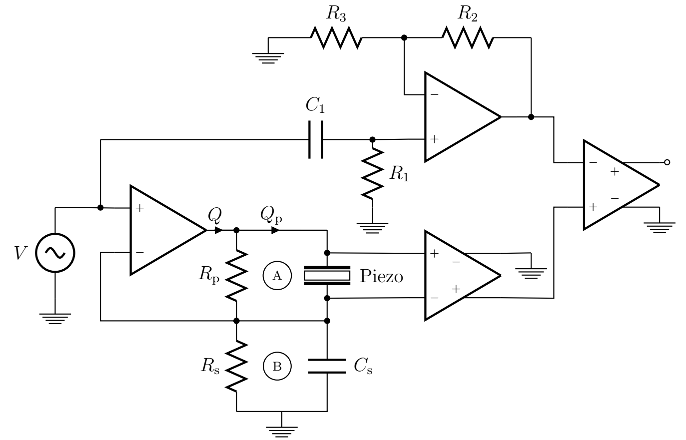

Fig. 7. Simplified circuit diagram of the piezoelectric cantilever in the charge driven - voltage measured setup.

4.2 Charge Actuation

The first amplifier stage shown in the lower branch of Fig. 7 was adopted from (Fleming and Moheimani, 2006) and used to drive the piezoelectric cantilever with a charge proportional to the input voltage. When the piezoelectric voltage V_p is neglected, the transfer function from reference voltage $V(s)$ to charge induced in the piezoelectric cantilever $Q_p(s)$ can be found by investigating the loops A and B as indicated in Fig. 7. From loop A it is found that

$$Q(s) = \frac{R_pC_ps+1}{R_pC_ps}Q_p(s) \tag{16}$$

and from loop B

$$Q(s) = \frac{C_sR_ss+1}{R_ss}V(s) \tag{17}$$

which, when equating (16) and (17), yields

$$Q_p(s) = H_{vq}(s)V(s) = \frac{R_pC_p}{R_s}\frac{C_sR_ss+1}{R_pC_ps+1}V(s). \tag{18}$$

For frequencies greater than $(2\pi R_pC_p)^{-1}$ and $(2\pi R_sC_s)^{-1}$ the circuit dynamics roll off and the piezoelectric cantilever is charge controlled. If additionally the values of the capacitors and resistors are chosen such that $C_pR_p = C_sR_s$, the poles and zeros in (18) cancel and a charge amplifier with gain C_s is obtained.

4.3 Feedthrough Cancellation

Examining the block diagram shown in Fig. 8 reveals the structure of the feedforward controller that is necessary to compensate the feedthrough term:

$$K(s) = \frac{H_{vq}(s)}{C_p} \tag{19}$$

The charge drive has been incorporated into the circuit shown in Fig. 7 with an analog feedforward controller and two instrumentation amplifiers. Parameters of the analog controller are obtained by fitting a first order high-pass filter to $H_{vq}(s)$. We note that with $G_{dv}(s)$ appearing in the feedback path of $G_{vq}(s)$, a shift of the resonance frequency is inherent to the system's properties. Compared to the constant changes of the resonance frequency of

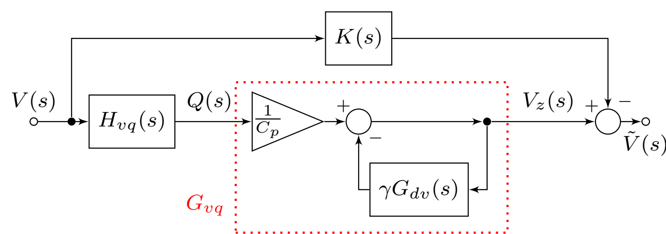

Fig. 8. Block diagram showing the schematic setup of charge actuation and feedthrough cancellation.

the cantilever during the operation of the atomic force microscope, this can be neglected.

5. EXPERIMENTAL RESULTS

5.1 Feedthrough Cancellation

Fig. 9 shows the measured frequency response of G_{qv} before and after feedthrough cancellation. It can be seen that the dynamic range is increased from less than 1 dB to more than 30 dB and the phase crosses $-90°$ at resonance and almost reaches $-180°$ after the resonance.

5.2 Noise Comparison

A noise comparison of the demodulated sensor signals around the resonance frequency is conducted with a Zürich Instruments lock-in amplifier HF2LI and shown in Fig. 10. The microcantilever is excited at its resonance with a peak voltage of 100 mV and the signal-to-noise ratio (SNR) is measured around a narrow bandwidth of 100 Hz. The SNR is determined to be the difference between the maximum value and the fitted noise floor and evaluates to approximately 131 dB for the laser signal and approximately 116 dB and 115 dB for the charge sensing and charge driving. The difference of approximately 15 dB can be attributed to limitations of the prototype analog circuitry and ambient noise sources.

5.3 Scan Results

Scan experiments with an NT-MDT NTEGRA Prima AFM on an NT-MDT TGZ1 calibration grating have been

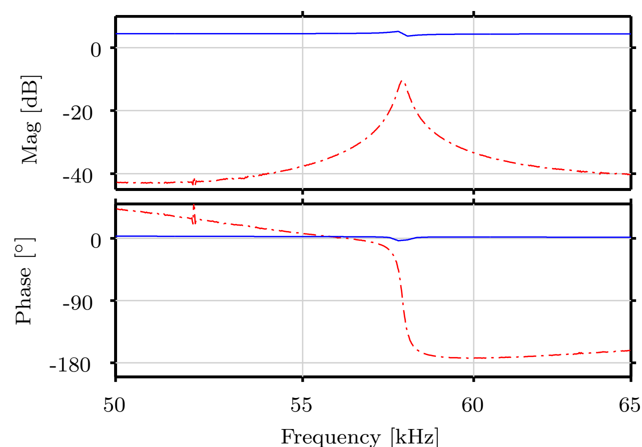

Fig. 9. Measured frequency response of G_{qv} without feedthrough cancellation (—) and with feedthrough cancellation (– · –).

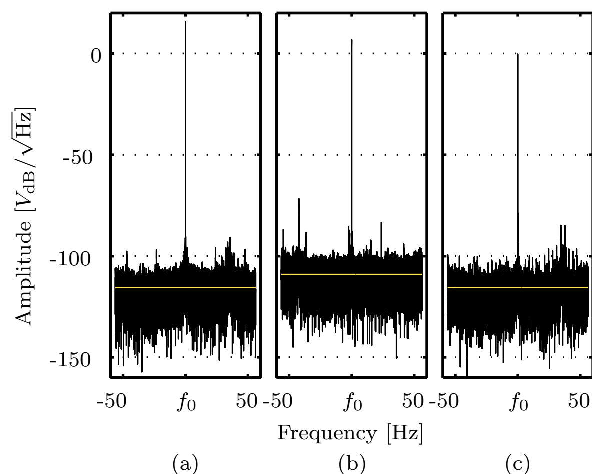

Fig. 10. Zoom-FFT of the deflection signal acquired from (a) the laser sensor, (b) the charge sensor and (c) the voltage sensor normalized around the resonance frequency. The horizontal yellow line indicates the fitted noise floor.

performed. The sample contains periodic features with step heights of 21.6 ± 1.5 nm. Fig. 11 shows the 2D and 3D images obtained with the laser signal and the deflection measurements from the self-sensing schemes. The scans were conducted over an area of 10 µm × 10 µm at a speed of 20 µm/s. The setpoint amplitude is kept at 50 % of the free-air amplitude. It can be concluded that under these equal scanning conditions the self-sensing methods yield very good image quality.

6. CONCLUSIONS

This work has highlighted how the optical deflection measurement system, which is normally employed in tapping-mode Atomic Force Microscopy, can easily be replaced with alternative sensing schemes when a piezoelectric cantilever is used. A single layer of piezoelectric material can be employed simultaneously for actuation and sensing using the relationship between charge, voltage and cantilever deflection. It was shown that even with a prototype implementation the sensors achieve excellent signal-to-noise ratio. The authors are currently working on an improved PCB design to further increase the SNR.

REFERENCES

Albrecht, T., Akamine, S., Carver, T.E., and Quate, C. (1990). Microfabrication of cantilever styli for the atomic force microscope. *J. Vac. Sci. Technol. A*, 8(4), 3386–3396.

Binnig, G., Quate, C.F., and Gerber, C. (1986). Atomic force microscope. *Phys. Rev. Lett.*, 56, 930–933.

Brogliato, B., Maschke, B., Lozano, R., and Egeland, O. (2007). *Dissipative Systems Analysis and Control*. Communications and Control Engineering. Springer-Verlag London.

Fairbairn, M.W. and Moheimani, S.O.R. (2012). Resonant control of an atomic force microscope micro-cantilever for active q control. *Review of Scientific Instruments*, 83(8), 083708–083708-9.

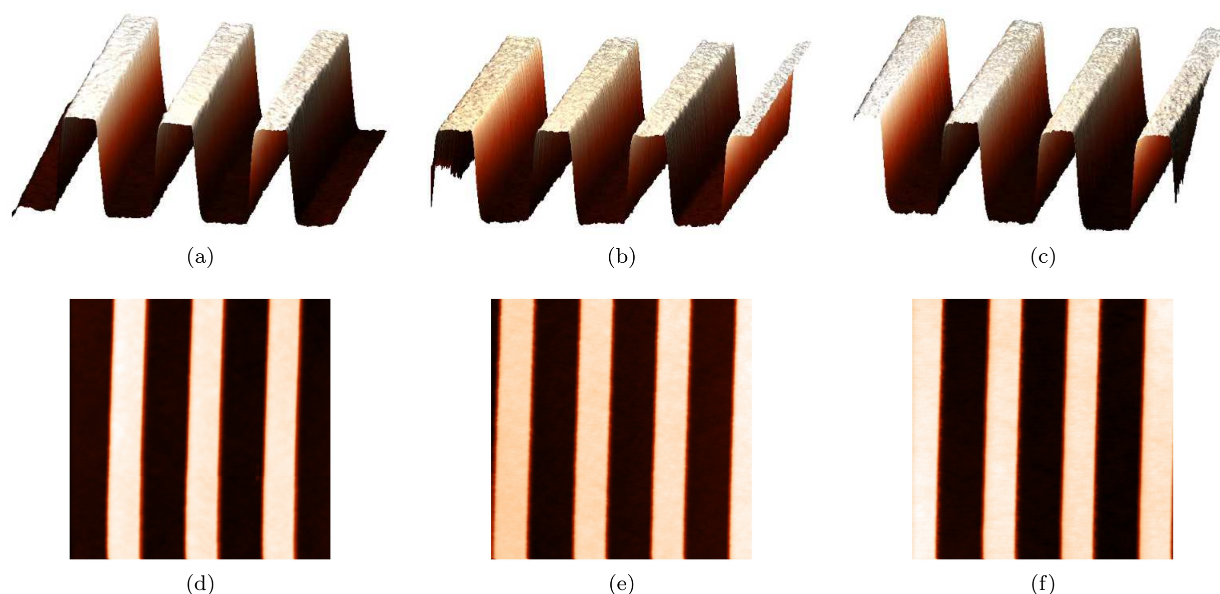

Fig. 11. 2D and 3D images obtained with (a),(d) the laser sensor; (b),(e) the voltage drive/ charge sensor and (c),(f) the charge drive/ voltage sensor.

Fanson, J. and Caughey, T.K. (1990). Positive position feedback control for large space structures. *AIAA Journal*, 28, 717–724.

Fantner, G.E., Schumann, W., Barbero, R.J., Deutschinger, A., Todorov, V., Gray, D.S., Belcher, A.M., Rangelow, I.W., and Youcef-Toumi, K. (2009). Use of self-actuating and self-sensing cantilevers for imaging biological samples in fluid. *Nanotechnology*, 20(43), 434003.

Fleming, A.J. and Moheimani, S.O.R. (2006). Sensorless vibration suppression and scan compensation for piezoelectric tube nanopositioners. *IEEE Trans. Contr. Syst. Technol.*, 14(1), 33–44.

Fleming, A.J. (2010). Nanopositioning system with force feedback for high-performance tracking and vibration control. *Mechatronics, IEEE/ASME Transactions on*, 15(3), 433–447.

Han, W., Lindsay, S.M., and Jing, T. (1996). A magnetically driven oscillating probe microscope for operation in liquids. *Appl. Phys. Lett.*, 69(26), 4111–4113.

Itoh, T. and Suga, T. (1993). Development of a force sensor for atomic force microscopy using piezoelectric thin films. *Nanotechnology*, 4(4), 218.

Kassies, R., van der Werf, K.O., Bennink, M.L., and Otto, C. (2004). Removing interference and optical feedback artifacts in atomic force microscopy measurements by application of high frequency laser current modulation. *Rev. Sci. Instrum.*, 75(3), 689–693.

Meitzler, A.H., Tiersten, H.F., Warner, A.W., Berlincourt, D., and Coquin, G.A. (1988). Ieee standard on piezoelectricity. *ANSI/IEEE Std 176-1987*.

Mertz, J., Marti, O., and Mlynek, J. (1993). Regulation of a microcantilever response by force feedback. *Appl. Phys. Lett.*, 62(19), 2344–2346.

Meyer, G. and Amer, N.M. (1988). Novel optical approach to atomic force microscopy. *Appl. Phys. Lett.*, 53(12), 1045–1047.

Moheimani, S.O.R. and Fleming, A.J. (2006). *Piezoelectric Transducers for Vibration Control and Damping.* Springer-Verlag London Limited.

Petersen, I. and Lanzon, A. (2010). Feedback control of negative-imaginary systems. *Control Systems, IEEE*, 30(5), 54–72.

Ruppert, M.G., Fairbairn, M.W., and Moheimani, S.O.R. (2013). Multi-mode resonant control of a microcantilever for atomic force microscopy. In *Proc. IEEE/ASME International Conference on Advanced Intelligent Mechatronics.* Wollongong, Australia.

Ruppert, M.G. and Moheimani, S.O.R. (2013). A novel self-sensing technique for tapping-mode atomic force microscopy. *Review of Scientific Instruments*, 84(12), 125006.

Tavassolizadeh, A., Meier, T., Rott, K., Reiss, G., Quandt, E., Hölscher, H., and Meyners, D. (2013). Self-sensing atomic force microscopy cantilevers based on tunnel magnetoresistance sensors. *Appl. Phys. Lett.*, 102(15), 153104.

Tortonese, M., Barrett, R.C., and Quate, C.F. (1993). Atomic resolution with an atomic force microscope using piezoresistive detection. *Appl. Phys. Lett.*, 62(8), 834–836.

Walters, D.A., Cleveland, J.P., Thomson, N.H., Hansma, P.K., Wendman, M.A., Gurley, G., and Elings, V. (1996). Short cantilevers for atomic force microscopy. *Rev. Sci. Instrum.*, 67(10), 3583–3590.

Yamanaka, K. and Nakano, S. (1996). Ultrasonic atomic force microscope with overtone excitation of cantilever. *Jpn. J. Appl. Phys.*, 35(Part 1, No. 6B), 3787–3792.

Yamashita, H., Kodera, N., Miyagi, A., Uchihashi, T., Yamamoto, D., and Ando, T. (2007). Tip-sample distance control using photothermal actuation of a small cantilever for high-speed atomic force microscopy. *Rev. Sci. Instrum.*, 78(8), 083702.

Zhong, Q., Inniss, D., Kjoller, K., and Elings, V. (1993). Fractured polymer/silica fiber surface studied by tapping mode atomic force microscopy. *Surf. Sci.*, 290(1-2), L688 – L692.